

ASMA: An Adaptive Safety Margin Algorithm for Vision-Language Drone Navigation via Scene-Aware Control Barrier Functions

Sourav Sanyal and Kaushik Roy

Electrical and Computer Engineering, Purdue University

{sanyals, kaushik}@purdue.edu

Abstract—In the rapidly evolving field of vision-language navigation (VLN), ensuring robust safety mechanisms remains an open challenge. Control barrier functions (CBFs) are efficient tools which guarantee safety by solving an optimal control problem. In this work, we consider the case of a teleoperated drone in a VLN setting, and add safety features by formulating a novel scene-aware CBF using ego-centric observations obtained through an RGB-D sensor. As a baseline, we implement a vision-language understanding module which uses the CLIP (Contrastive Language Image Pretraining) model to query about a user-specified (in natural language) landmark. Using the YOLO (You Only Look Once) object detector, the CLIP model is queried for verifying the cropped landmark, triggering downstream navigation. To improve navigation safety, we propose an Adaptive Safety Margin Algorithm (ASMA) – that crops the drone’s depth map for tracking moving object(s) to perform scene-aware CBF evaluation on-the-fly. By identifying potential risky observations from the scene, ASMA enables real-time adaptation to unpredictable environmental conditions, ensuring optimal safety bounds on a VLN-powered drone actions. Using the robot operating system (ROS) middleware on a parrot bebop2 quadrotor in the Gazebo environment, ASMA offers 59.4% - 61.8% increase in success rates with insignificant 5.4% - 8.2% increases in trajectory lengths compared to the baseline CBF-less VLN while recovering from unsafe situations.

I. INTRODUCTION

Foundational models pretrained on exa-scale internet data have made significant strides in vision and language processing tasks requiring little to no fine-tuning as exemplified by a new family of AI models such as BERT [1], GPT-3 [2], GPT-4 [3], CLIP [4], DALL-E [5] and PALM-E [6], to name a few. The fusion of vision and language models [4], [6] have enabled machines to interact with operating environments in increasingly intuitive ways. As these models become more widespread, the once sci-fi dream of robots understanding and interacting in complex environments through natural language commands is now a reality. This transformation is made possible by the recently emerging field of vision-language navigation (VLN) [7]–[12].

Autonomous drones which have the ability to assist in smart agriculture, carry out search and rescue as well as respond to fire hazards [13] are becoming increasingly ubiquitous. Drones are predicted to contribute up to \$54.6 billion to the global economy by 2030 [14]. We envision a future where teleoperated drones will be able to translate human-specified contextual instructions into low-level actions which a machine can execute, while navigating through unfamiliar

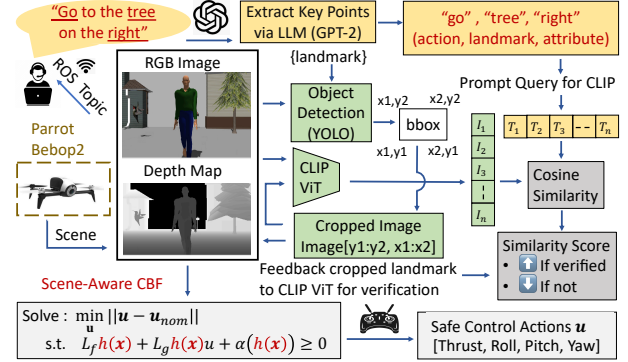


Fig. 1. Overview of the ASMA framework, integrating CLIP for vision-language understanding, YOLO for object detection, and scene-aware CBFs via cropped depth-map for safe vision-language drone navigation.

dynamic environments using robot vision. In this regard, as we embark into industry 4.0 [15], VLN models for teleoperated drones offer exciting possibilities. However, ensuring safety and reliability for VLN in drones is still an open research problem. Control barrier functions (CBFs) [16], [17] provide a mathematical framework for maintaining safety constraints in dynamical systems, making them useful for real-time applications where safety is crucial. To that effect, we propose ASMA, an adaptive safety margin algorithm for VLN in drones. By formulating a novel scene-aware CBF, ASMA robustifies a drone VLN model. Implemented on a parrot bebop2 quadrotor with an RGB-D sensor in the Gazebo environment [18]–[20], a baseline VLN first uses a large language model (LLM) to identify navigation landmarks. Then it integrates CLIP (for scene understanding) with YOLO (for object detection [21]) using the robot operating system (ROS) middleware. This enables the model to query about landmarks and detect objects. Subsequently, ASMA identifies risky observations along the baseline drone VLN’s path by processing ego-centric depth maps to dynamically evaluate scene-aware CBFs. This results in a hybrid approach utilizing AI as well as symbolic rules which adjusts the control commands of a VLN-powered drone using formal safety methods emerging from control theory. The main contributions of this work are as follows:

- We implement a vision-language understanding module (VLUM) using a CLIP-based YOLO detection framework to function as a drone VLN (Section III-A).
- We propose scene-aware CBFs (SA-CBFs) that adjust

drone commands based on real-time operator as well as environmental feedback, improving robustness against dynamic obstacles (Section III-B).

- We integrate VLUM and SA-CBF using ROS, by implementing thread synchronization between CLIP and YOLO to avoid deadlock (Section III-C).
- We provide a detailed analysis showing significant improvements in navigation accuracy and safety when ASMA is applied to a baseline CBF-less VLN method on a parrot bebop2 quadrotor in Gazebo (Section IV).

To the best of our knowledge, this is the first work which integrates CBFs with VLN, robustifying high-level vision-language understanding with low-level CBFs for a downstream autonomous navigation task.

II. RELATED WORK

Vision-Language Models for Robot Navigation: In Vision-Language Navigation (VLN), agents interpret language commands to navigate through environments using visual cues [7]–[12]. Previous works, such as [8], [9], have expanded VLN into continuous environments (VLN-CE). Works in [10]–[12] have explored VLN focusing on interpreting visually-grounded instructions and developing models like VLN BERT to improve navigation performance through entity-landmark pre-training techniques. [22] employs 2D LiDAR for safer waypoint prediction in VLN-CE, while [23], [24] integrate pretrained visual-language features with navigation maps. The work in [25] utilizes action prompts for improved spatial navigation precision. Room2Room [26] enables teleoperated communication using augmented reality, and [27] introduces the ‘Tryout’ method to prevent collision-related navigational stalls. However, these approaches do not address the physical dynamics of robots, crucial for verifying safety. Our work focuses on a teleoperated drone similar to [28] with VLN capabilities, utilizing an RGB-D sensor and aims to enhance its safety and reliability in dynamic environments.

Control Barrier Functions for Safety: Control barrier functions (CBFs) are essential tools from robust control theory, ensuring safety constraints are maintained in dynamic systems [16], [17]. By defining safe boundaries through mathematical functions, CBFs dynamically adjust control actions to prevent safety violations. Vision-based control barrier functions (V-CBFs) [29] extend these safety protocols to unknown environments, using conditional generative adversarial networks (C-GAN). Differentiable control barrier functions (dCBFs) integrated into neural networks via BarrierNet [30] offer end-to-end trainable safety layers adaptable to environmental changes. Additionally, [31] develops a low-cost method for synthesizing quadratic CBFs over point cloud data, improving safe navigation. Visual locking CBFs (VCBF) and parametrizable switching descending CBFs (DCBF) further support precise drone landing safety [32].

III. PROPOSED APPROACH

In this work, we deploy the parrot bebop2 quadrotor within a ROS-powered Gazebo environment, following [18]–[20], equipped with an RGB-D sensor for VLN tasks. We propose ASMA – an Adaptive Safety Margin Algorithm for drone VLN using a novel scene-aware CBF formulation. Figure 1 provides a high-level overview. The following sections detail the functional blocks of ASMA.

A. Vision-Language Understanding Module (VLUM)

We utilize the CLIP model [4] to design our vision-language understanding module (VLUM) by mapping images and text into a shared embedding space, which allows effective comparison between visual data and textual descriptions. The CLIP model has separate encoders for images Φ_{img} and texts Φ_{text} . The operator views images from a ROS topic and issues a command like "Go to the tree on the right." We use the GPT-2 LLM to parse this command into key components: the action ("go to"), the landmark ("tree"), and the attribute ("on the right"). Given the input image \mathbf{I} , the YOLO object detection function $\mathbf{D}_{\text{YOLO}}(\mathbf{I})$ outputs a bounding box $\mathbf{bbox} = (x_1, y_1, x_2, y_2, l)$ for the detected landmark l , using which we extract the cropped image \mathbf{I}_{crop} from the original image \mathbf{I} .

$$\mathbf{bbox} = \mathbf{D}_{\text{YOLO}}(\mathbf{I}) \quad (1a)$$

$$\mathbf{I}_{\text{crop}} = \text{CropImage}(\mathbf{I}, \mathbf{bbox}) \quad (1b)$$

This cropped image is then processed by the CLIP model’s image encoder Φ_{img} to verify the landmark. The similarity score \mathbf{S} is calculated by measuring the cosine similarity between the embeddings of the original and cropped images with respect to the text prompt \mathbf{T} .

$$\mathbf{T} = \text{"This is a rendering of a"} + l \quad (2)$$

$$\mathbf{S}_{\text{scene}} = \frac{\Phi_{\text{img}}(\mathbf{I}) \cdot \Phi_{\text{text}}(\mathbf{T})}{\|\Phi_{\text{img}}(\mathbf{I})\| \cdot \|\Phi_{\text{text}}(\mathbf{T})\|} \quad (3a)$$

$$\mathbf{S}_{\text{landmark}} = \frac{\Phi_{\text{img}}(\mathbf{I}_{\text{crop}}) \cdot \Phi_{\text{text}}(\mathbf{T})}{\|\Phi_{\text{img}}(\mathbf{I}_{\text{crop}})\| \cdot \|\Phi_{\text{text}}(\mathbf{T})\|} \quad (3b)$$

The relationship between the similarity score \mathbf{S} and the drone’s operations can be interpreted as follows:

- If $\mathbf{S}_{\text{landmark}} > \mathbf{S}_{\text{scene}}$, the landmark is correctly identified within the drone’s field of view (FoV).
- If $\mathbf{S}_{\text{landmark}} < \mathbf{S}_{\text{scene}}$, the landmark may no longer be in the FoV, indicating the drone has moved away.

These dynamics ensure that \mathbf{S} triggers appropriate downstream navigational tasks when verified. A decrease in \mathbf{S} prompts the operator to issue a new VLN instruction.

Fine-Tuning the CLIP Model: The pre-trained CLIP model, robust for broad vision-language tasks suffers a domain shift in our 3D Gazebo simulation environment due to the wide nature of the images it has been pretrained on. To address this domain shift, we incorporated a custom attention layer that dynamically adjusts focus on relevant image regions

based on the input text prompts. This was achieved through a query-key-value (QKV) attention mechanism, where attention scores A_{att} are computed to indicate the relevance of different image regions to the text. Let \mathbf{F}_{img} and \mathbf{F}_{text} represent the image and text features, respectively:

$$Q = W_q \cdot \mathbf{F}_{\text{text}}, \quad K = W_k \cdot \mathbf{F}_{\text{img}}, \quad V = W_v \cdot \mathbf{F}_{\text{img}} \quad (4)$$

Here, the text features generate the query vector Q , while the image features generate the key and value vectors K and V . The attention scores A_{att} , computed as:

$$A_{\text{att}} = \text{Softmax} \left(\frac{Q \cdot K^T}{\sqrt{d_k}} \right) \cdot V, \quad (5)$$

determine the degree of focus applied to different image regions. W_q , W_k , and W_v are learnable weight matrices, and d_k is the dimensionality of the key vectors. The resulting attention scores are used to compute the attended image features $\mathbf{F}_{\text{att-img}}$:

$$\mathbf{F}_{\text{att-img}} = \sum_i A_{\text{att}}^i \cdot \mathbf{F}_{\text{img}}^i, \quad (6)$$

which highlight the parts of the image most relevant to the text prompt. The model is trained using a contrastive loss function $\mathcal{L}_{\text{contrastive}}$, defined as:

$$\mathcal{L}_{\text{contrastive}} = \sum_{i=1}^N \left(\log \frac{\exp(\langle F_i^{\text{att-img}}, F_i^{\text{text}} \rangle / \tau)}{\sum_{j=1}^N \exp(\langle F_i^{\text{att-img}}, F_j^{\text{text}} \rangle / \tau)} \right),$$

where $\langle F_i^{\text{att-img}}, F_i^{\text{text}} \rangle$ is the dot product between the attended image features and text embeddings for positive pairs, and the denominator considers all pairs. The temperature τ is a hyperparameter that controls the scaling. This QKV attention mechanism is applied across two training stages, following a curriculum learning approach.

Stage 1 (Cropped Landmark Fine-Tuning): The attention mechanism focuses on cropped landmarks detected by YOLO, improving text-object alignment by assigning attention to relevant cropped regions of the prompted landmarks.

Stage 2 (Whole Scene Fine-Tuning): The attention mechanism is applied to whole scenes, enabling the model to distinguish landmarks within a broader context while ignoring background noise. Training with the contrastive loss ensures semantic alignment of landmarks within the scene based on their textual descriptions.

By training in both stages, the model generalizes from isolated landmarks to complex scenes, improving landmark identification during inference. The attention mechanism allows ASMA to focus on relevant image regions based on text prompts, enabling accurate navigation in real time.

B. Enhancing VLUM with Formal Safety Methods

Control barrier functions (CBFs) are essential tools in safety-critical control systems that enforce safety constraints through mathematical functions.

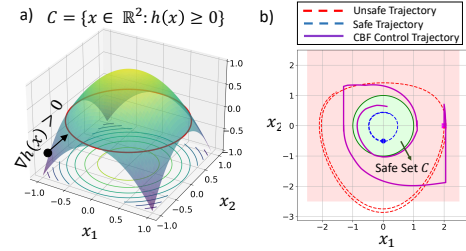


Fig. 2. Toy Illustration of Control Barrier Functions. (a) 3D view of the safe set C where $h(x) \geq 0$ (above red ring). (b) Comparison of trajectories: unsafe (red dashed), safe (blue dashed), and CBF-controlled (magenta solid).

1) **Preliminaries:** We consider a quadrotor described by the following non-linear control affine dynamics with an ego-centric depth-map:

$$\dot{x} = f(x) + g(x)u, \quad \xi = \Psi(x, d) \quad (7)$$

Here, \dot{x} denotes the time derivative of the state vector $x \in \mathbb{R}^{12}$, covering the drone's positions, orientations, and velocities. The control input $u \in \mathbb{R}^4$, consists of thrust, roll, pitch, and yaw. Functions $f(x)$ form the autonomous dynamics and $g(x)$ signifies the dynamics that can be controlled in an affine manner. Additionally, the depth-map d provides obstacle distances, with $\xi = \Psi(x, d)$ transforming these distances from pixel to physical space, incorporating the drone's current position. Let $C \subset \mathbb{R}^{12}$ represent a *safety set* defined through a continuously differentiable function $h(x)$ such that:

$$C = \{x \in \mathbb{R}^{12} : h(x) \geq 0\} \quad (8)$$

Figure 2a illustrates a toy safety set C , marked by the boundary where $h(x) = 0$ and the region where $h(x) > 0$, indicating safe operational zones. The function $h(x)$ is characterized by its lie derivatives:

$$L_f h(x) = \nabla h(x) \cdot f(x), \quad (9a)$$

$$L_g h(x) = \nabla h(x) \cdot g(x), \quad (9b)$$

which are critical for monitoring the system's safety relative to state changes and control action changes.

Theorem (Safety Verification): For safety verification, it is required that:

$$L_f h(x) + L_g h(x)u + \alpha(h(x)) \geq 0, \quad (10)$$

where α is a class \mathcal{K} function (meaning $\alpha(0) = 0$ and $\alpha(\mathcal{K}x_2) > \alpha(\mathcal{K}x_1) \forall x_2 > x_1$ and $\mathcal{K} > 0$). $\nabla h(x) > 0$ in the unsafe region ($h(x) < 0$) will drive $h(x)$ to become positive again.

Corollary (Adaptive Control): If a function $h(x)$ can be designed such that adjustments in u continuously satisfy the constraint in Eqn. (10), the system's response adapts dynamically to environmental changes while ensuring safety.

This forms the core of our Scene-Aware CBF control:

$$\min_u J(u) = \min_u \|u - u_{\text{nom}}\| \quad (11)$$

where the objective is to minimize a cost function $J(u)$ quantifying the deviation from a nominal control input u_{nom}

Algorithm 1 Scene-Aware CBF

```

1: function SA-CBF( $\mathbf{p}_{\text{curr}}, \mathbf{p}_{\text{target}}, \mathbf{u}_{\text{nom}}, \text{Obstacles}$ )
2:    $\vec{\mathbf{d}}_{\text{target}} = \vec{\mathbf{p}}_{\text{target}} - \vec{\mathbf{p}}_{\text{curr}}$ 
3:   for each obstacle in Obstacles do
4:      $\vec{\mathbf{d}}_{\text{obs}} = \vec{\mathbf{p}}_{\text{obs}} - \vec{\mathbf{p}}_{\text{curr}}$ 
5:     Compute  $h(\mathbf{x})$  using Equation 15
6:     if  $h(\mathbf{x}) < 0$  then
7:        $\sigma \leftarrow \text{sign}((\vec{\mathbf{d}}_{\text{target}} \times \vec{\mathbf{d}}_{\text{obs}})_z)$ 
8:        $\mathbf{u}_{\text{new}} \leftarrow \arg \min J(\mathbf{u})$ 
9:         s.t.  $L_f h(\mathbf{x}) + L_g h(\mathbf{x})\mathbf{u} + \alpha(h(\mathbf{x})) \geq 0$ 
10:         $\cap \sigma \cdot \text{yaw\_rate}(\mathbf{u}) \geq 0$ 
11:       return  $\mathbf{u}_{\text{new}}$ 
12:     else
13:       return  $\mathbf{u}_{\text{nom}}$ 
14:     end if
15:   end for
16: end function

```

satisfying Eqn. (10). This ensures that in case there is a safety violation, adaptive control drives the system from the unsafe state back within the safe set \mathcal{C} , as shown in the toy example in Figure 2b, making \mathcal{C} a forward invariant set.

2) *Navigation Direction*: Depth map points are converted into 3D coordinates $\boldsymbol{\xi} = \Psi(\mathbf{x}, \mathbf{D}_{\text{crop}})$ relative to the drone’s body frame using intrinsic camera parameters:

$$X_c = (i - c_x) \cdot \frac{d}{f}, \quad Y_c = (j - c_y) \cdot \frac{d}{f}, \quad Z_c = d \quad (12)$$

i and j denote pixel coordinates, d is the depth at those coordinates from the cropped depth maps \mathbf{D}_{crop} , f is the focal length, and c_x, c_y are the center coordinates of the camera. These local coordinates (X_c, Y_c, Z_c) are then transformed into the global frame:

$$\begin{bmatrix} X_g & Y_g & Z_g \end{bmatrix}^\top = \mathbf{R} \cdot \begin{bmatrix} X_c & Y_c & Z_c \end{bmatrix}^\top + \vec{\mathbf{p}}_{\text{curr}} \quad (13)$$

using a rotation matrix (\mathbf{R}) and current drone position $\vec{\mathbf{p}}_{\text{curr}} = [x, y, z]$. The transformation function $\boldsymbol{\xi} = \Psi(\mathbf{x}, \mathbf{d})$ facilitates navigation by integrating depth map data to enhance the detection of targets and obstacles, providing coordinates for dynamic planning. $\vec{\mathbf{d}}_{\text{target}}$ and $\vec{\mathbf{d}}_{\text{obs}}$ are the direction vectors to the estimated waypoint and obstacle respectively:

$$\vec{\mathbf{d}}_{\text{target}} = \vec{\mathbf{p}}_{\text{target}} - \vec{\mathbf{p}}_{\text{curr}}, \quad (14a)$$

$$\vec{\mathbf{d}}_{\text{obs}} = \vec{\mathbf{p}}_{\text{obs}} - \vec{\mathbf{p}}_{\text{curr}}. \quad (14b)$$

$\sigma = \text{sign}((\vec{\mathbf{d}}_{\text{target}} \times \vec{\mathbf{d}}_{\text{obs}})_z)$ is defined as the sign of the cross product of the vectors along the z axis. $\sigma > 0$ or $\sigma < 0$ indicates obstacles situated to right or left respectively.

3) *Scene-Aware CBF*: The proposed Scene-Aware Control Barrier Function (SA-CBF) is defined as:

$$h(\mathbf{x}) = \begin{bmatrix} \vec{\mathbf{d}}_{\text{obs}} - \mathbf{d}_{\text{safe}} \\ \theta - \theta_{\text{safe}} \end{bmatrix} \quad (15)$$

$$\theta = \cos^{-1} \left(\frac{\vec{\mathbf{d}}_{\text{target}} \cdot \vec{\mathbf{d}}_{\text{obs}}}{\|\vec{\mathbf{d}}_{\text{target}}\| \|\vec{\mathbf{d}}_{\text{obs}}\|} \right) \quad (16)$$

Algorithm 2 Adaptive Safety Margin Algorithm (ASMA)

```

Input: RGB-D image  $\mathbf{I}$ , VLN instruction  $\text{cmd}$ 
Output: Drone command vector  $\mathbf{u}$  with safety bounds
1: Initialize global_image, global_depth from RGB-D
2: while not ROSPY.IS_SHUTDOWN() do
3:    $\text{cmd\_parsed} \leftarrow \text{LLM}(\text{cmd})$ 
4:   Start Thread A:
5:   Acquire image_lock ▷ Wait for I
6:    $\text{bbox} \leftarrow \text{DYOLO}(\text{global\_img})$ 
7:    $\mathbf{I}_{\text{crop}} \leftarrow \text{CropImage}(\text{global\_img}, \text{bbox})$ 
8:    $\mathbf{D}_{\text{crop}} \leftarrow \text{CropDepth}(\text{global\_depth}, \text{bbox})$ 
9:   Release image_lock
10:  Start Thread B:
11:  Acquire image_lock ▷ Wait for I,  $\mathbf{I}_{\text{crop}}$ 
12:   $\mathbf{E}_{\text{img}} \leftarrow \Phi_{\text{img}}(\mathbf{I})$ 
13:   $\mathbf{E}_{\text{crop}} \leftarrow \Phi_{\text{img}}(\mathbf{I}_{\text{crop}})$ 
14:   $\mathbf{E}_{\text{txt}} \leftarrow \Phi_{\text{txt}}(\text{cmd\_parsed})$ 
15:   $\mathbf{S}_{\text{scene}} \leftarrow \text{COMP\_SIM}(\mathbf{E}_{\text{img}}, \mathbf{E}_{\text{txt}})$ 
16:   $\mathbf{S}_{\text{landmark}} \leftarrow \text{COMP\_SIM}(\mathbf{E}_{\text{crop}}, \mathbf{E}_{\text{txt}})$ 
17:  Release image_lock
18:  Sync_Thread(A,B)
19:  if  $\mathbf{S}_{\text{landmark}} > \mathbf{S}_{\text{scene}}$  then
20:     $\mathbf{u} \leftarrow \text{SA-CBF}(\mathbf{p}_{\text{curr}}, \mathbf{p}_{\text{target}}, \mathbf{u}_{\text{nom}}, \mathbf{h}(\mathbf{x}), \text{Obstacles})$ 
21:    PUBLISH_CONTROL( $\mathbf{u}$ ) ▷ Send  $\mathbf{u}$  to actuators
22:  else
23:    Issue new VLN instruction  $\text{cmd}$ 
24:  end if
25: end while

```

θ is the angle between $\vec{\mathbf{d}}_{\text{obs}}$ and $\vec{\mathbf{d}}_{\text{target}}$. Gradients for each component of $h(\mathbf{x})$ are given by:

$$\nabla h_1(\mathbf{x}) = \sigma_d \cdot \partial \vec{\mathbf{d}}_{\text{obs}} / \partial \mathbf{x}, \quad (17a)$$

$$\nabla h_2(\mathbf{x}) = -\csc \theta \cdot \partial \cos \theta / \partial \mathbf{x}. \quad (17b)$$

σ_d indicates the gradient direction for maintaining or increasing distance from obstacles. The gradients calculate changes in the directions which help compute the lie derivatives in Eqn. (10) guiding the optimization process to adjust the control actions. In addition to Eqn. (10), the cost function $J(\mathbf{u})$ in Eqn. (11) is subjected to the directional constraint

$$\sigma \cdot \text{yaw_rate}(\mathbf{u}) \geq 0 \quad (18)$$

as an added variant. We call this ASMA-Steering as it imposes an explicit directional signal as a hard constraint.

C. Adaptive Safety Margin Algorithm (ASMA)

The process starts with system setup and ongoing shutdown signal monitoring (Algorithm 2, lines 1-2). VLN instructions are interpreted (line 3), and two threads handle image data. Thread A focuses on object detection, identifying landmarks and adjusting image focus areas (lines 5-9). Concurrently, thread B encodes the cropped images and compares them with the parsed instructions to verify the landmarks (lines 11-17). After synchronizing the threads (line 18), the algorithm evaluates if the landmarks align with the drone’s navigation objectives (line 19). If a landmark is appropriately aligned, SA-CBF (Algorithm 1) is applied to adjust the control strategy using depth data (line 21). This drives the drone while adapting to environmental changes.



Fig. 3. Gazebo snapshots for 4 VLN commands with ASMA-steering. See the video for better visualization. The drone has been marked in a circle.

IV. RESULTS

A. Methodology

We implemented the ASMA framework in ROS on a parrot bebop2 quadrotor within the Gazebo environment. The pretrained CLIP model from OpenAI's repository [33], was fine-tuned with huggingface's template [34], using pyTorch [35]. Object detection was performed using YOLOv5 [36] (~ 21 million parameters), with training data annotated via LabelImg [37]. The pretrained CLIP consisted of ~ 149 million parameters. Because of the large model sizes, we performed thread synchronization (Algorithm 2) to toggle between the two inference modes. Text descriptions for CLIP fine-tuning were generated using [38]. We collected ~ 1800 image-text pairs, 1000 of which were used for fine-tuning and 800 for evaluating the fine-tuned model. The CLIP model was fine-tuned at a learning rate of $1e - 04$ for 4 epochs in Stage 1 and for 8 epochs with early stopping in Stage 2 [39]. The temperature τ was set to 0.2. Scene-Aware CBF optimizations were conducted using cvxopt [40], and the RotorS simulator [41] was used to integrate lower level control. \vec{d}_{safe} was set to 2 meters and θ_{safe} to 30 degrees. RGB-D sensor focal length f was set to 10 meters.

B. Comparative Schemes

- **CBF-less VLN:** The baseline scenario which lacks CBF safety features.
- **ASMA:** Implements scene-aware CBFs based on the constraint in Equation (10).
- **ASMA-Steering:** Extends ASMA by adding the directional constraint from Equation (18).

For evaluating vision-language understanding performance, we use similarity scores S_{scene} and $S_{\text{landmarks}}$. For navigation performance, we use three metrics: a) Trajectory Length (TL), b) Success Rate (SR) — the percentage of times the drone ended within 1 meter of the destination, and c) Navigation Error (NE) — the linear distance between the target and the actual endpoint of the flight path.

C. Vision-Language Understanding Performance

Table I shows the similarity scores for both whole scenes and cropped landmarks, with and without fine-tuning. Two improvements are observed: 1) the increase from whole scene to cropped landmarks, and 2) the increase from pretrained to fine-tuned models. For example, in ResNet-50, the "tree"

TABLE I

SIMILARITY SCORE BEFORE AND AFTER LOCATING OBJECTS. CLIP IS THE PRETRAINED MODEL AND CLIP-FT IS A FINE-TUNED MODEL.

Vision Subsystem		"tree"		"house"		"mailbox"	
		CLIP	CLIP -FT	CLIP	CLIP -FT	CLIP	CLIP -FT
ResNet -50	Whole Scene	0.24	0.54	0.23	0.43	0.21	0.48
	Cropped	0.27	0.87	0.26	0.87	0.29	0.93
ViT -B/16	Whole Scene	0.35	0.64	0.31	0.51	0.23	0.59
	Cropped	0.43	0.82	0.35	0.91	0.28	0.93
ViT -B/32	Whole Scene	0.33	0.58	0.31	0.59	0.28	0.52
	Cropped	0.42	0.89	0.37	0.94	0.36	0.89

score improves from 0.24 (whole scene) to 0.27 (cropped), and after fine-tuning, it rises from 0.54 to 0.87. Similarly, in ViT-B/16, the "tree" score improves from 0.35 (whole scene) to 0.43 (cropped), and from 0.64 to 0.82 after fine-tuning. YOLO-cropped images generally yield higher scores than whole scenes across all encoders. ViT-B/16, with its 16x16 patches, processes features in more detail than ViT-B/32 with 32x32 patches. Fine-tuning mitigates the domain shift between pretrained CLIP and the 3D Gazebo world, aligning the model better with the environment. The similarity scores, ranging from -1 to 1, reflect reasonable performance in the zero-shot setting. Please note fine-tuning is necessary for generating relevant captions for the end-user. However, even without fine-tuning, the increase in similarity scores for cropped objects still triggers downstream navigation, guiding the drone to the target locations (see Figure 3).

D. Vision-Language Navigation Performance

Table II presents the Vision-Language Navigation (VLN) performance across different methods, with Figure 4 visualizing the corresponding trajectories for four VLN commands. The results show that the CBF-less method consistently achieves lower success rates (SR) across all commands, as the lack of safety constraints increases the likelihood of navigation failures. ASMA significantly improves SRs, increasing from $\sim 61\%$ to $\sim 92\%$ for the first command, with a slightly higher trajectory length (TL) of 8.60 compared to 8.54 for the CBF-less method, indicating a small detour for safety. ASMA-Steering further enhances navigation by reducing navigation errors (NE), such as lowering NE from 1.23 in ASMA to 0.96 in ASMA-Steering for the second command, with SR increasing to $\sim 91\%$. On average, ASMA increases the SR by 59.4% compared to the CBF-less method (from

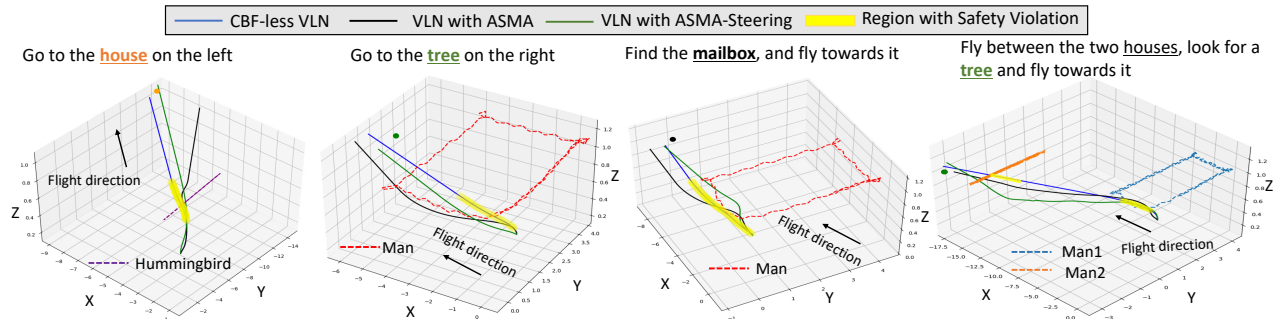


Fig. 4. Simulated Trajectories for 4 VLN commands for baseline and two variants of ASMA. Distances are in meters. Moving objects have dashed lines.

TABLE II
PERFORMANCE OF 4 VLN INSTRUCTIONS FOR 3 VLN METHODS. \uparrow OR \downarrow INDICATES WHETHER INCREASE OR DECREASE IS BETTER.

VLN Instruction	VLN Method	TL \downarrow	SR \uparrow	NE \downarrow
Go to the house on the left (cmd1)	CBF-Less	8.54	61.01	2.80
	ASMA	8.60	92.19	3.11
	ASMA-Steering	8.52	91.82	2.40
Go to the tree on the right (cmd2)	CBF-Less	4.64	55.59	1.21
	ASMA	5.41	90.08	1.23
	ASMA-Steering	4.85	92.49	0.96
Find the mailbox, and fly towards it (cmd3)	CBF-Less	5.24	55.32	2.01
	ASMA	6.17	91.18	2.01
	ASMA-Steering	6.27	91.47	1.83
Fly between the two houses, look for a tree and fly towards it (cmd4)	CBF-Less	14.51	50.81	0.51
	ASMA	14.70	91.41	0.50
	ASMA-Steering	18.82	93.03	0.36

57.18% to 91.19%), with a minor 5.4% increase in TL (from 8.23 to 8.67), reflecting the slight safety detour. ASMA-Steering further improves SR by 61.8% while increasing TL by only 8.2% on average, with further decrease in NE.

E. Adaptive Safety Margins

ASMA dynamically modulates control actions based on calculated safety margins $h(x)$, which determine the drone's proximity to obstacles. This process, shown in Figure 5 (for the ASMA-Steering variant) using the distance component of $h(x)$ operates in three zones. In Zone 1 (Safe Operation), where $h(x)[0] > 0$, the drone operates under standard flight parameters without needing obstacle avoidance adjustments. In Zone 2 (Potential Risk), when $h(x)[0] \leq 0$, ASMA adjusts the drone's trajectory and reduces speed to mitigate risks, represented by the red zone in Figure 5. Finally, in Zone 3 (Safety Restoration), after encountering an obstacle, ASMA restores standard flight controls, with a slightly delayed transition if directional constraints are absent (not shown in Figure 5). This showcases ASMA's adaptability in maintaining safety across various VLN tasks.

V. SUMMARY

In this work, we introduced ASMA (Adaptive Safety Margin Algorithm) to robustify VLN for teleoperated drones using a novel scene-aware CBF. We implemented a VLN model on a parrot bebop2 quadrotor utilizing CLIP for scene

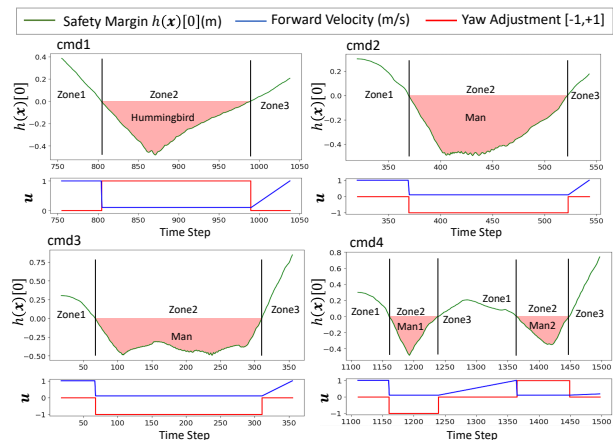


Fig. 5. Illustration of ASMA-Steering for 4 VLN instructions. When obstacle is far, CBF value > 0 indicates safe operation (Zone1). When obstacle is near, CBF value < 0 indicates potential risk (Zone2) triggering ASMA to drive the system back to safe state with CBF value > 0 (Zone3). CBF value is first element of $h(x)$ in meters. Velocity varies between 0 to 1 m/s. Yaw is normalized between -1 and +1.

understanding and YOLO for object detection in Gazebo. ASMA adjusts control actions using real-time depth data ensuring safe navigation in complex environments. Two ASMA variants improved success rates of a baseline CBF-less VLN method by 59.4% and 61.8% on average with slight trajectory increases as safety detours.

Note, in this work we used object detection to locate landmarks and obstacles as one possible perception method in the CLIP-based VLN setting, assuming the wide-spread availability of open-world detection datasets. However, for outdoor navigation or path-planning, segmentation could identify navigable regions as well. ASMA can be extended to support segmentation and other modalities, hence serving as a framework for enforcing VLN safety through scene-aware CBFs across a wide range of perception techniques. ASMA combines AI with formal safety methods from control theory that can (hopefully) serve as a template for improving safety and reliability in next-generation cognitive system design.

VI. ACKNOWLEDGEMENT

This work was supported by the Center for the Co-Design of Cognitive Systems (CoCoSys), a center in JUMP 2.0, an SRC program sponsored by DARPA.

REFERENCES

- [1] J. Devlin, "Bert: Pre-training of deep bidirectional transformers for language understanding," *arXiv preprint arXiv:1810.04805*, 2018.
- [2] T. Brown, B. Mann, and *et al.*, "Language models are few-shot learners," *Advances in Neural Information Processing Systems*, vol. 33, pp. 1877–1901, 2020.
- [3] J. Achiam, S. Adler, S. Agarwal, L. Ahmad, I. Akkaya, F. L. Aleman, D. Almeida, J. Altenschmidt, S. Altman, S. Anadkat *et al.*, "Gpt-4 technical report," *arXiv preprint arXiv:2303.08774*, 2023.
- [4] A. Radford, J. W. Kim, C. Hallacy, A. Ramesh, G. Goh, S. Agarwal, G. Sastry, A. Askell, P. Mishkin, J. Clark *et al.*, "Learning transferable visual models from natural language supervision," in *International conference on machine learning*. PMLR, 2021, pp. 8748–8763.
- [5] A. Ramesh, M. Pavlov, G. Goh, S. Gray, C. Voss, A. Radford, M. Chen, and I. Sutskever, "Zero-shot text-to-image generation," in *International conference on machine learning*. Pmlr, 2021, pp. 8821–8831.
- [6] D. Driess, F. Xia, M. S. Sajjadi, C. Lynch, A. Chowdhery, B. Ichter, A. Wahid, J. Tompson, Q. Vuong, T. Yu *et al.*, "Palm-e: An embodied multimodal language model," *arXiv preprint arXiv:2303.03378*, 2023.
- [7] D. Shah, B. Osiński, S. Levine *et al.*, "Lm-nav: Robotic navigation with large pre-trained models of language, vision, and action," in *Conference on robot learning*. PMLR, 2023, pp. 492–504.
- [8] J. Krantz, E. Wijmans, A. Majumdar, D. Batra, and S. Lee, "Beyond the nav-graph: Vision-and-language navigation in continuous environments," in *Computer Vision—ECCV 2020: 16th European Conference, Glasgow, UK, August 23–28, 2020, Proceedings, Part XXVIII 16*. Springer, 2020, pp. 104–120.
- [9] Y. Hong, Z. Wang, Q. Wu, and S. Gould, "Bridging the gap between learning in discrete and continuous environments for vision-and-language navigation," in *Proceedings of the IEEE/CVF Conference on Computer Vision and Pattern Recognition*, 2022, pp. 15 439–15 449.
- [10] P. Anderson, Q. Wu, D. Teney, J. Bruce, M. Johnson, N. Sünderhauf, I. Reid, S. Gould, and A. Van Den Hengel, "Vision-and-language navigation: Interpreting visually-grounded navigation instructions in real environments," in *Proceedings of the IEEE conference on computer vision and pattern recognition*, 2018, pp. 3674–3683.
- [11] Y. Hong, Q. Wu, Y. Qi, C. Rodriguez-Opazo, and S. Gould, "Vln bert: A recurrent vision-and-language bert for navigation," in *Proceedings of the IEEE/CVF conference on Computer Vision and Pattern Recognition*, 2021, pp. 1643–1653.
- [12] Y. Cui, L. Xie, Y. Zhang, M. Zhang, Y. Yan, and E. Yin, "Grounded entity-landmark adaptive pre-training for vision-and-language navigation," in *Proceedings of the IEEE/CVF International Conference on Computer Vision*, 2023, pp. 12 043–12 053.
- [13] F. Giones and A. Brem, "From toys to tools: The co-evolution of technological and entrepreneurial developments in the drone industry," *Business Horizons*, vol. 60, no. 6, pp. 875–884, 2017.
- [14] DroneII, "Drone market report," 2024. [Online]. Available: https://droneii.com/product/drone-market-report?srsltid=AfmBOor-qVivIWByTvlyTvfvT_ZNWT1ZJJ7N52-1K0j_4QoQ0cImOEUI
- [15] M. Ghebakhloo, "Industry 4.0, digitization, and opportunities for sustainability," *Journal of cleaner production*, vol. 252, p. 119869, 2020.
- [16] A. D. Ames, S. Coogan, M. Egerstedt, G. Notomista, K. Sreenath, and P. Tabuada, "Control barrier functions: Theory and applications," in *2019 18th European control conference (ECC)*. IEEE, 2019, pp. 3420–3431.
- [17] A. D. Ames, X. Xu, J. W. Grizzle, and P. Tabuada, "Control barrier function based quadratic programs for safety critical systems," *IEEE Transactions on Automatic Control*, vol. 62, no. 8, pp. 3861–3876, 2016.
- [18] S. Sanyal and K. Roy, "Ramp-net: A robust adaptive mpc for quadrotors via physics-informed neural network," in *2023 IEEE International Conference on Robotics and Automation (ICRA)*. IEEE, 2023, pp. 1019–1025.
- [19] S. Sanyal, R. K. Manna, and K. Roy, "Ev-planner: Energy-efficient robot navigation via event-based physics-guided neuromorphic planner," *IEEE Robotics and Automation Letters*, 2024.
- [20] A. Joshi, S. Sanyal, and K. Roy, "Real-time neuromorphic navigation: Integrating event-based vision and physics-driven planning on a parrot bebop2 quadrotor," *arXiv preprint arXiv:2407.00931*, 2024.
- [21] T. Diwan, G. Anirudh, and J. V. Tembhurne, "Object detection using yolo: Challenges, architectural successors, datasets and applications," *multimedia Tools and Applications*, vol. 82, no. 6, pp. 9243–9275, 2023.
- [22] L. Yue, D. Zhou, L. Xie, F. Zhang, Y. Yan, and E. Yin, "Safe-vln: Collision avoidance for vision-and-language navigation of autonomous robots operating in continuous environments," *IEEE Robotics and Automation Letters*, 2024.
- [23] C. Huang, O. Mees, A. Zeng, and W. Burgard, "Visual language maps for robot navigation," in *2023 IEEE International Conference on Robotics and Automation (ICRA)*. IEEE, 2023, pp. 10 608–10 615.
- [24] Z. Wang, X. Li, J. Yang, Y. Liu, and S. Jiang, "Gridmm: Grid memory map for vision-and-language navigation," in *Proceedings of the IEEE/CVF International Conference on Computer Vision*, 2023, pp. 15 625–15 636.
- [25] B. Lin, Y. Zhu, Z. Chen, X. Liang, J. Liu, and X. Liang, "Adapt: Vision-language navigation with modality-aligned action prompts," in *Proceedings of the IEEE/CVF Conference on Computer Vision and Pattern Recognition*, 2022, pp. 15 396–15 406.
- [26] T. Pejša, J. Kantor, H. Benko, E. Ofek, and A. Wilson, "Room2room: Enabling life-size telepresence in a projected augmented reality environment," in *Proceedings of the 19th ACM conference on computer-supported cooperative work & social computing*, 2016, pp. 1716–1725.
- [27] D. An, H. Wang, W. Wang, Z. Wang, Y. Huang, K. He, and L. Wang, "Etnpav: Evolving topological planning for vision-language navigation in continuous environments," *IEEE Transactions on Pattern Analysis and Machine Intelligence*, 2024.
- [28] R. Ibrahimov, E. Tsykunov, V. Shirokun, A. Somov, and D. Tsetserukou, "Dronepick: Object picking and delivery teleoperation with the drone controlled by a wearable tactile display," in *2019 28th IEEE International conference on robot and human interactive communication (RO-MAN)*. IEEE, 2019, pp. 1–6.
- [29] H. Abdi, G. Raja, and R. Ghabcheloo, "Safe control using vision-based control barrier function (v-cbf)," in *2023 IEEE International Conference on Robotics and Automation (ICRA)*. IEEE, 2023, pp. 782–788.
- [30] W. Xiao, T.-H. Wang, R. Hasani, M. Chahine, A. Amini, X. Li, and D. Rus, "BarrierNet: Differentiable control barrier functions for learning of safe robot control," *IEEE Transactions on Robotics*, vol. 39, no. 3, pp. 2289–2307, 2023.
- [31] M. De Sa, P. Kotaru, and K. Sreenath, "Point cloud-based control barrier function regression for safe and efficient vision-based control," in *2024 IEEE International Conference on Robotics and Automation (ICRA)*. IEEE, 2024, pp. 366–372.
- [32] V. N. Sankaranarayanan, A. Saradagi, S. Satpute, and G. Nikolakopoulos, "A cbf-adaptive control architecture for visual navigation for uav in the presence of uncertainties," *arXiv preprint arXiv:2402.10729*, 2024.
- [33] OpenAI, "Clip: Connecting text and images," <https://github.com/openai/CLIP>, 2021.
- [34] H. Face, "Hugging face model hub," <https://huggingface.co/models>, 2021.
- [35] A. Paszke, S. Gross, F. Massa, A. Lerer, J. Bradbury, G. Chanan, T. Killeen, Z. Lin, N. Gimelshein, L. Antiga *et al.*, "Pytorch: An imperative style, high-performance deep learning library," 2019. [Online]. Available: <https://pytorch.org>
- [36] Ultralytics, "Yolov5: Object detection at 640x640," <https://github.com/ultralytics/yolov5>, 2020.
- [37] Tzatalin, "Labelimg," <https://github.com/tzatalin/labelImg>, 2020.
- [38] T. Wolf, J. Chaumond, L. Debut, V. Sanh, C. Delangue, A. Moi, P. Cistac, M. Funtowicz, J. Davison, S. Shleifer, and *et al.*, "Transformers: State-of-the-art natural language processing," in *Proceedings of the 2020 Conference on Empirical Methods in Natural Language Processing: System Demonstrations*. Association for Computational Linguistics, 2020, pp. 38–45.
- [39] L. Prechelt, "Early stopping - but when?" in *Neural Networks: Tricks of the Trade, volume 1524 of LNCS, chapter 2*. Springer-Verlag, 1997, pp. 55–69.
- [40] M. S. Andersen, J. Dahl, and L. Vandenberghe, "Cvxopt: Python software for convex optimization," <https://cvxopt.org>, 2021.
- [41] F. Furrer, M. Burri, M. Achtelik, and R. Siegwart, *Robot Operating System (ROS): The Complete Reference (Volume 1)*. Cham: Springer International Publishing, 2016, ch. RotorS—A Modular Gazebo MAV Simulator Framework, pp. 595–625.